Polymer Bulletin (2026) 83:244
https://doi.org/10.1007/s00289-026-06303-x

ORIGINAL PAPER

3D printing of olive pit powder–reinforced PVA/HAp scaffolds: a sustainable strategy for bone tissue engineering

Mohamed Bella Jagitay[1,2] · Gulpembe Ustundag[1,3] · Zehra Desen Celik[1,4] · Ayse Onur[1,5] · Tuba Bedir[1] · Sena Su Torun[1,6] · Elif Ilhan[1] · Oguzhan Gunduz[1,7]

Received: 1 September 2025 / Revised: 8 January 2026 / Accepted: 12 January 2026
© The Author(s) 2026

Abstract

The development of sustainable, biocompatible scaffolds for bone tissue engineering is crucial to address the limitations of conventional grafting approaches. In this study, we report the fabrication and characterization of 3D-printed scaffolds composed of polyvinyl alcohol (PVA), olive pith powder (OPP), and hydroxyapatite (HAp) using an extrusion-based technique. Four different formulations (1PVA/0OPP/HAp, 1PVA/1OPP/HAp, 2PVA/5OPP/HAp, and 5PVA/2OPP/HAp) were evaluated to investigate the effects of varying PVA-OPP ratios on the structural, mechanical, and biological properties of the scaffolds. FTIR analysis confirmed the successful incorporation of OPP and HAp into the PVA matrix through the retention of characteristic functional groups and enhanced hydrogen bonding. SEM analysis revealed that increasing OPP content improved inter-pore connectivity and surface roughness, with pore sizes ranging from ~382 to ~572 μm, which is ideal for osteogenesis. Mechanical testing demonstrated a balance between stiffness and ductility depending on OPP concentration. The 1PVA/0OPP/HAp scaffold exhibited the highest tensile strength and modulus, while the 1PVA/1OPP/HAp group showed superior strain capacity. Cytocompatibility assessed by MTT assay and fluorescent staining showed that moderate OPP content (1PVA/1OPP/HAp and 5PVA/2OPP/HAp) promoted cell viability and spreading, while excessive OPP (2PVA/5OPP/HAp) impaired proliferation, possibly due to phenolic compound-induced oxidative stress. These results suggest that OPP can serve as a promising, sustainable filler in bone tissue engineering scaffolds when used at optimized concentrations.

Keywords 3D printing · Olive pit powder · Polyvinyl alcohol · Hydroxyapatite · Bone tissue engineering · Sustainable biomaterials

Extended author information available on the last page of the article

Published online: 02 February 2026

Introduction

Bone tissue serves as a crucial structural component of the human body [1], accounting for approximately 15% of total body weight and functioning as the primary support system for vital organs and mobility [2, 3]. It also plays a dynamic role in calcium homeostasis, hematopoiesis, and endocrine regulation [4]. However, critical-sized bone defects caused by trauma, tumors, infections such as osteomyelitis, or congenital conditions remain a major challenge in clinical orthopedics and maxillofacial surgery [5]. The intrinsic regenerative capacity of bone is often insufficient for repairing such defects, necessitating the development of effective bone graft substitutes [5, 6]. Conventional strategies for bone repair, including autografts, allografts, and xenografts, are commonly employed in clinical settings [7]. However, these approaches are often associated with notable limitations, such as limited donor availability, postoperative complications at the donor site, immune rejection, and the risk of pathogen transmission [8]. Therefore, there is an increasing demand for bone graft substitutes that are safe, effective, and readily available [9]. In this context, tissue engineering has emerged as a promising field, aiming to develop biomimetic scaffolds that facilitate bone regeneration.

Scaffolds play a central role in tissue engineering by providing a temporary 3D matrix that supports cell adhesion, proliferation, and differentiation while guiding new tissue formation [10]. An ideal scaffold for bone tissue engineering must exhibit biocompatibility, osteoconductivity, appropriate mechanical strength, and a controlled degradation profile [10, 11]. Additionally, it should possess a hierarchical porous architecture with interconnected macropores (> 100 μm) for vascular ingrowth and micropores (< 10 μm) to support cell attachment and nutrient diffusion [12]. Despite significant progress, conventional scaffolds often fail to achieve these criteria simultaneously, highlighting the need for new, multifunctional, and sustainable biomaterials.

Conventional fabrication methods for bone scaffolds, including freeze-drying, solvent casting, and electrospinning, often suffer from limited control over pore architecture, batch-to-batch variability, and restricted tunability of mechanical properties [13]. In contrast, extrusion-based 3D printing offers a versatile platform for the layer-by-layer fabrication of scaffolds with controlled geometry, porosity, and architecture in a reproducible and customizable manner [14]. This technique is particularly suitable for incorporating complex composite materials, allowing the integration of bioactive and structural components into a single platform [15]. 3D-printed scaffolds can be engineered with spatially controlled porosity and mechanical characteristics to mimic the anisotropic properties of natural bone [16].

In recent years, increasing attention has been given to the use of agro-industrial byproducts in scaffold fabrication due to their cost-effectiveness, biodegradability, and low environmental impact [17]. Among these, olive pit powder (OPP), a byproduct of the olive oil industry, has demonstrated potential as a natural filler or reinforcement in composite materials. Rich in cellulose, hemicellulose, and lignin, OPP exhibits thermal stability, natural porosity, and inherent biocompatibility [18, 19]. Its incorporation into composite materials also aligns with principles of circular

economy and green chemistry, promoting resource efficiency and environmental sustainability [20, 21].

To enhance the structural and biological properties of OPP-based scaffolds, their combination with polymers such as polyvinyl alcohol (PVA) has been explored. PVA is a water-soluble synthetic polymer known for its excellent film-forming capability, biocompatibility, and mechanical stability in hydrated environments [22, 23]. Blending PVA with OPP enables the fabrication of composite inks suitable for extrusion-based 3D printing while maintaining sufficient integrity and printability. Moreover, this approach improves the scaffold's mechanical properties and supports the formation of a porous architecture ideal for bone tissue applications [24, 25].

Further enhancement in bioactivity can be achieved by incorporating hydroxyapatite (HAp), a naturally occurring calcium phosphate mineral that closely resembles the inorganic component of bone. HAp is widely recognized for its osteoconductive and osteoinductive properties, promoting bone cell attachment, proliferation, and mineralization [26, 27]. When integrated into polymer-based scaffolds, HAp improves not only the mechanical stiffness but also the biological performance, accelerating bone tissue regeneration in vitro and in vivo [28–30]. To the best of our knowledge, this is the first study to systematically investigate the integration of OPP, an agricultural waste from the circular economy, into 3D-printed PVA/HAp scaffolds using extrusion-based bioprinting for bone tissue engineering applications.

In this study, we developed and characterized 3D-printed scaffolds composed of PVA, OPP, and HAp using extrusion-based printing. Four different formulations, 1PVA/0OPP/HAp, 1PVA/1OPP/HAp, 2PVA/5OPP/HAp, and 5PVA/2OPP/HAp, were prepared to investigate the effects of varying polymer-to-biomass ratios on scaffold performance. The fabricated scaffolds were evaluated in terms of their chemical, morphological, and mechanical properties and in vitro cytocompatibility via MTT assay. This study aims to contribute to the development of sustainable, cost-effective, and biologically functional scaffolds for bone tissue engineering by combining biowaste valorization with additive manufacturing technologies (Fig. 1).

Materials and methods

Preparation of Olive pit powder (OPP)

The synthesis of OPP (Biolive, Istanbul, Türkiye) hydrogel commenced with the preparation of a sodium hydroxide (NaOH; Sigma-Aldrich, USA) solution at room temperature. A 3 M NaOH solution was prepared at room temperature by dissolving in distilled water under moderate stirring to ensure homogeneity. OPP was gradually added to the NaOH solution at a concentration of 10% (w/v) and stirred continuously at 750–1000 rpm for 2 h using a magnetic stirrer to achieve uniform dispersion and partial dissolution of the biomass. To remove residual NaOH, the resulting OPP hydrogel was subjected to membrane dialysis. Dialysis tubing was pre-soaked in distilled water and then filled with the OPP solution. After sealing, the dialysis bags were immersed in 1 L of distilled water and maintained at room temperature for 72 h,

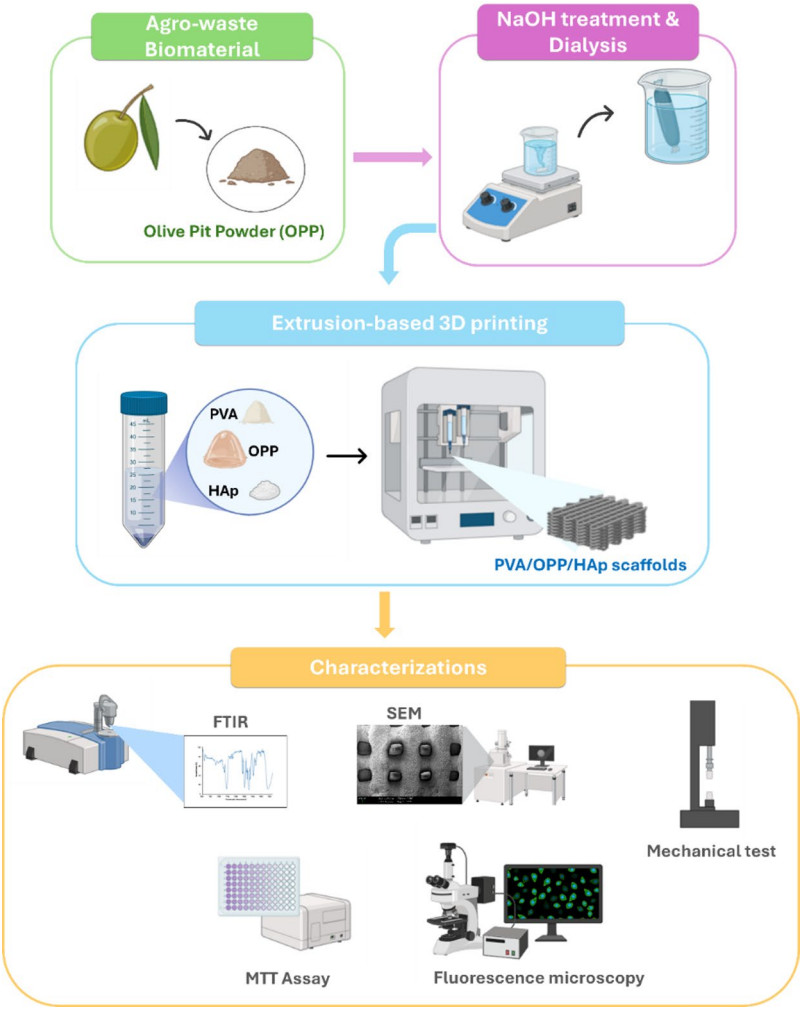


Fig. 1 Schematic illustration of the fabrication and characterization of 3D-printed PVA/OPP/HAp scaffolds for bone tissue engineering applications

with the water being refreshed twice daily (every 8–12 h). The dialyzed hydrogel was stored in sealed tubes at +4 °C until further use.

Preparation of PVA/OPP/HAp composite formulations

A 25% (w/v) solution of polyvinyl alcohol (PVA; M_w = 89,000–98,000, 99+% hydrolyzed, Sigma Aldrich, Darmstadt, Germany) was prepared by dissolving PVA in distilled water at 90 °C for 2 h under constant stirring. Four different PVA-to-OPP ratios were formulated: 1:1, 2:5, 5:2, and 1:0 (PVA only), with the latter serving as the control group. The PVA and OPP mixtures were subjected to a single freeze–thaw cycle for physical crosslinking by freezing at −20 °C for 2 h, followed by thawing at room

temperature for 2 h. This limited cycle was employed to prevent excessive crosslinking and maintain desirable mechanical properties. Following the freeze–thaw process, the mixtures were weighed, and hydroxyapatite (HAp; ≥ 90%, Sigma Aldrich, Darmstadt, Germany) was incorporated at a concentration of 20% (w/w) using an emulsion-based method to ensure homogeneous distribution within the PVA/OPP matrix.

The PVA-to-OPP ratios were selected to systematically assess the influence of polymer composition and lignocellulosic content on scaffold structure, mechanical behavior, and biological response. The 1:0 formulation (PVA only) served as the control group to isolate the effect of OPP incorporation, while the 1:1 ratio represented a balanced composite system. The 2:5 and 5:2 ratios were designed to explore OPP-dominant and PVA-dominant systems, respectively, allowing evaluation of matrix continuity, filler dispersion, and intermolecular interactions across a broad compositional spectrum.

3D printing of PVA/OPP/HAp composite scaffolds

The scaffolds were designed using PrusaSlicer software, and corresponding G-codes were generated for fabrication. Each scaffold was designed with dimensions of 30 mm × 30 mm × 5 mm. Fabrication was carried out using an AXO-1 pressure extrusion-based 3D printer equipped with an 18-gauge tip. A 12 mL volume of the prepared solution was loaded into the printer's syringe reservoir to construct scaffolds.

Fourier transform infrared (FTIR) spectroscopy

Fourier transform infrared spectroscopy (FTIR) was employed to analyze the chemical composition of the 3D-printed OPP/PVA/HAp scaffolds. FTIR spectra were recorded using a JASCO FT/IR-4700 spectrometer within the wavenumber range of 4000–400 cm^{-1}, at a resolution of 4 cm^{-1}.

Scanning electron microscopy (SEM)

The morphological characteristics of the 3D-printed scaffolds were examined using a scanning electron microscope (SEM; EVA MA 10, Zeiss, Jena, Germany). Before imaging, the scaffolds were coated with a thin layer of gold using a sputter coater (Quorum SC7620, UK).

Mechanical testing

Tensile testing was performed to evaluate the mechanical properties of the 3D-printed scaffolds. Uniaxial tensile tests were conducted using a Shimadzu EZ-LX universal testing machine equipped with a 5 kN load cell. The tests were carried out at room temperature with a constant crosshead speed of 5 mm/min. Rectangular scaffold specimens with defined dimensions (20 mm × 10 mm) were prepared for testing. At least $n = 3$ samples were tested for each group to ensure statistical reliability. Ten-

sile strength, Young's modulus, and elongation at break were calculated from the obtained stress–strain curves.

Cell culture and cytocompatibility assessment

DMEM-F12 (Dulbecco's Modified Eagle Medium-F12 (Capricorn)) was used to cultivate the human osteoblastic cell line (hFOB, ATCC-CRL-3602) in a 5% CO_2 incubator at 37 °C (ThermoFisher). Trypsin/EDTA (Gibco) was used to separate the cells once they had attained about 80% confluency in the flask. A suitable volume of DMEM-F12 was used to lyse the cell pellet that resulted from centrifuging the collected cells for five minutes at 2000 rpm. A cell counting equipment (Anvajo Science) was used to determine the total number of cells.

To assess cell viability, the materials were meticulously cut into 6-mm diameter discs and sterilized by UV irradiation for 2 h. After sterilization, the materials were rinsed with phosphate-buffered saline (PBS) and subsequently placed into a 96-well plate. Each well was filled with complete culture medium (DMEM-F12), supplemented with 10% fetal bovine serum (FBS, Biowest) and 1% penicillin/streptomycin (Gibco), and the materials were incubated for 24 h to allow for stabilization. hFOB cells were seeded onto the materials at an initial concentration of 1×10^4 cells per well. The same number of cells was also seeded into empty wells as a 2D control. The cell-seeded materials were incubated at 37 °C in 5% CO_2 for 7 days. To evaluate cell proliferation, an MTT (3-(4,5-Dimethylthiazol-2-yl)-2,5-Diphenyltetrazolium Bromide) (ElabScience) assay was performed. MTT solution was added to the samples on days 1, 3, and 7 post-seeding. After 3 h of incubation, DMSO was added to the wells to form formazan crystals, and the results were evaluated at 570 nm with a microplate reader (Multiskan SkyHigh, ThermoScientific). Cell viability was calculated using the following formula (1):

$$\text{Viability } (\%) = \left(\frac{ODs}{ODc}\right) \times 100 \tag{1}$$

where *ODs* refers to the average optical density measured for the scaffolds, while *ODc* refers to the average optical density measured for the negative control. All experimental conditions were conducted in triplicate to ensure the robustness and reproducibility of the results.

Fluorescence microscopy analysis

Fluorescence microscopy analysis was performed to examine the adhesion of hFOB cells on the scaffolds. For this examination, cells on scaffolds seeded with hFOB cells were fixed on day 3 and then labeled with Alexa Fluor 488 phalloidin (Invitrogen) and DAPI (Invitrogen) dyes. Alexa Fluor Phalloidin binds to actin filaments, allowing visualization of the cytoskeleton and actin filaments. DAPI is a DNA-specific dye that binds to the DNA of cell nuclei, allowing easy visualization of DNA and live cell nuclei. During the analysis process, the samples were washed with PBS after remov-

ing the 3-day growth medium. Then, the cells were fixed with 4% formaldehyde and stained using Alexa Fluor 488 phalloidin and DAPI supplied by Thermofisher. The examination of the prepared materials was performed using a fluorescence microscope (Evos, ThermoScientific).

Results and discussion

ourier transform infrared (FTIR) spectroscopy

The spectra for HAp, OPP, PVA components, and the 3D-printed OPP/PVA/HAp scaffolds at varying ratios are presented in Fig. 2. The FTIR spectrum of the pure HAp displayed characteristic sharp peaks at around 1022, 962, and 603–560 cm^{-1} corresponding to the asymmetric and symmetric stretching and bending modes of PO_4^{3-} ions. These agree with the typical HAp signature reported in the literature [31, 32]. The spectrum of OPP exhibited absorption bands typical of lignocellulosic compounds. The broad band between 3400 and 3300 cm^{-1} corresponds to O–H stretching vibrations from hydroxyl groups [33]. The peak around 2900 cm^{-1} is associated with the –CH group of cellulose, hemicellulose, and lignin [34], while the band at around 1635 cm^{-1} is assigned to C = O stretching [35]. Additionally, the peak at around 1033 cm^{-1} represents the C–O stretching in cellulose and hemicellulose, which are abun-

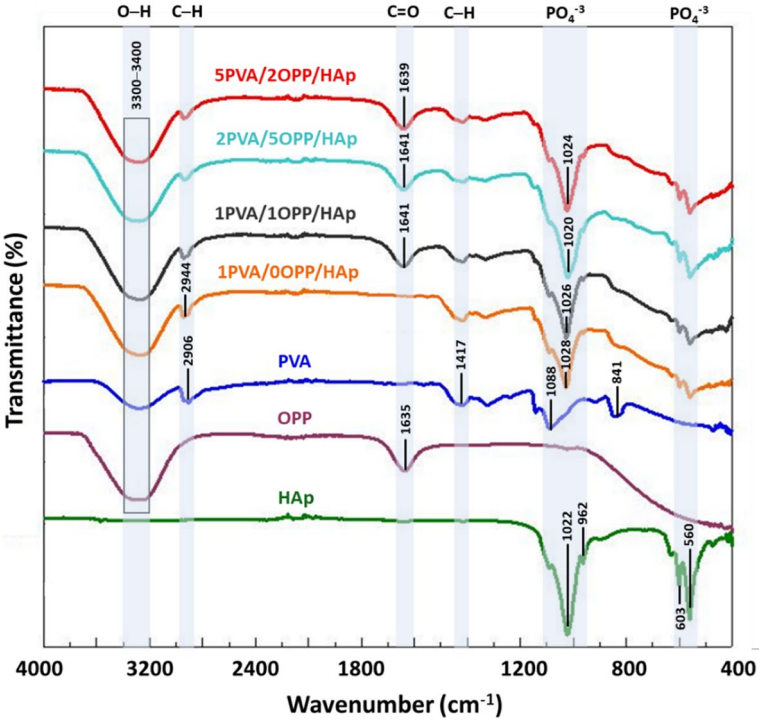


Fig. 2 FTIR spectra of HAp, OPP, PVA components, and the 3D-printed PVA/OPP/HAp scaffolds

dant in olive-derived biomass [34, 35]. For pure PVA, the characteristic absorption bands at 3275, 2906, and 1417 cm^{-1} are attributed to O–H stretching, C–H stretching of alkyl groups, and C–H bending vibrations, respectively [36]. The C–O stretching vibration is observed around 1088 cm^{-1}, while the band at 841 cm^{-1} corresponds to C–C stretching vibrations [37]. FTIR spectra for the 1PVA/1OPP/HAp, 2PVA/5OPP/HAp, and 5PVA/2OPP/HAp composite scaffolds reveal the retention of key absorption bands from each component, indicating the effective incorporation of both OPP and HAp into the PVA matrix. Notably, the broadening of the O–H stretching band in the 3270–3280 cm^{-1} range suggests enhanced hydrogen bonding between the hydroxyl groups of PVA and the lignocellulosic structures present in OPP. Such interactions are known to promote the formation of physically crosslinked crystalline domains in freeze–thaw-treated PVA systems, thereby influencing mechanical stability and degradation behavior [38]. Moreover, the presence of phosphate-related peaks (1030–560 cm^{-1}) in all composite spectra confirms the successful integration of HAp into the scaffold formulations. This indicates that HAp preserves its crystalline phase during scaffold fabrication, acting as a nucleating agent within the polymeric matrix. These findings are also in good agreement with previous reports in the literature [30, 37, 39].

Morphological analysis

SEM analysis was employed at varying magnifications (50×, 100×, and 5000×) to assess the morphological characteristics of the 3D-printed scaffolds across various PVA/OPP/HAp formulations. As shown in Fig. 3, the porosity, surface texture, and filament integrity vary notably with changes in the PVA: OPP: HAp ratio. The 1PVA/0OPP/HAp scaffold exhibits irregular pore architecture, with partially collapsed pore walls and inconsistent filament deposition. The average pore diameter is approximately 312 µm, which falls within the lower end of the optimal range for bone tissue applications. The surface appears relatively smooth at higher magnification, a characteristic feature of pure PVA-based systems attributed to their hydrophilic nature [36]. The absence of OPP may have contributed to the limited viscosity and shape accuracy during extrusion-based printing. With the addition of OPP, the architecture of the 1PVA/1OPP/HAp scaffold becomes more pronounced with uniform strand deposition and improved pore interconnectivity; it exhibits approximately 382 µm pore size. High-magnification imaging reveals agglomerated OPP particles embedded within the matrix, contributing to an increased surface roughness [33]. Such surface roughness has been shown to promote cellular adhesion and proliferation, consistent with previous findings on scaffolds reinforced with lignocellulosic fillers [40, 41]. 2PVA/5OPP/HAp scaffold, where the OPP content is significantly increased, exhibits the largest pore size, around 572 µm, and a highly regular grid-like pattern. This suggests a favourable balance between viscosity and filler content, enabling sufficient flow during extrusion while maintaining scaffold integrity. The pore size in this scaffold aligns well with the recommended range of ≥ 300 µm for promoting osteogenesis, vascularization, and osteoblast migration [3], which may enhance cell infiltration and new tissue formation. Moreover, the microscale roughness observed at 5000× confirms the presence of abundant filler particles, which can

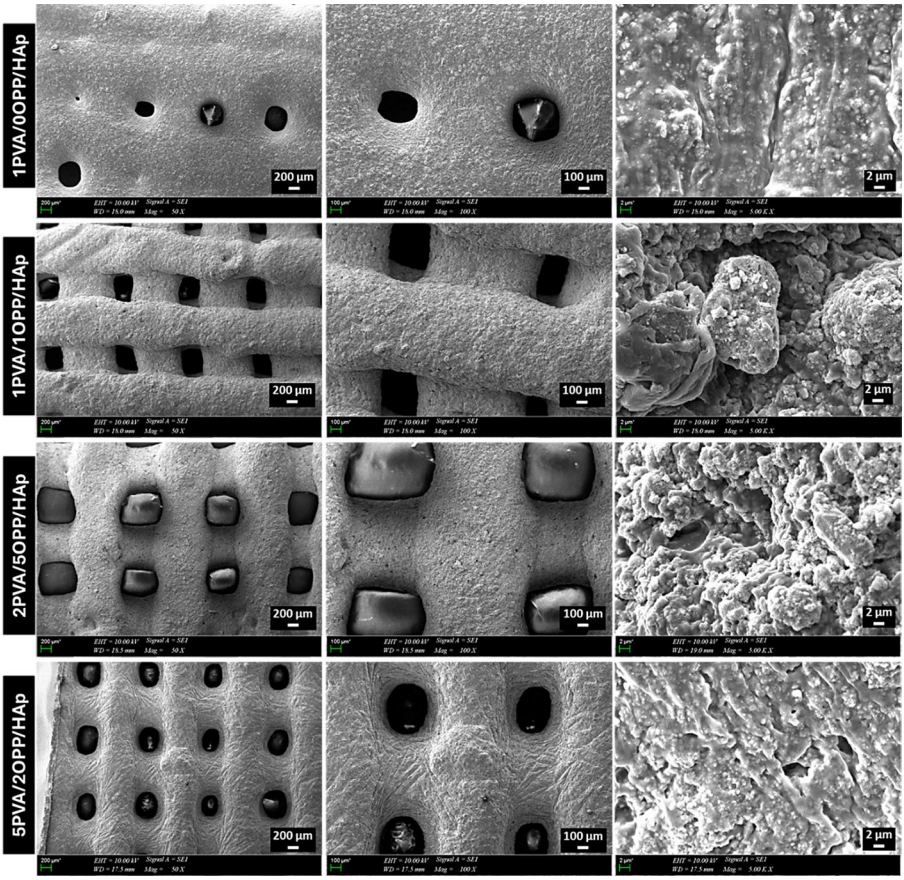


Fig. 3 SEM images of 3D-printed 1PVA/0OPP/HAp, 1PVA/1OPP/HAp, 2PVA/5OPP/HAp, and 5PVA/2OPP/HAp scaffolds

enhance mechanical integrity and osteoconductive properties [42]. Increasing PVA content further in the 5PVA/2OPP/HAp scaffold led to a slight reduction in pore size to about 428 µm. Despite its high structural uniformity and smoother architecture, the increased viscosity of the polymer solution may have restricted pore expansion, limiting diffusion pathways. However, the circular and evenly spaced pores still provide an adequate microenvironment for early-stage bone regeneration [43]. At high magnification (5000×), the surface appears dense with a mildly fibrous morphology, where both HAp and OPP particles are uniformly embedded within the matrix. This microstructural arrangement resembles the native bone extracellular matrix, which may facilitate cell attachment and promote osteogenic activity [44]. Overall, increasing OPP content improves the structural fidelity, surface roughness, and possibly the mechanical performance of the scaffolds. The inclusion of HAp further contributes to bioactivity, as evidenced by the granular structures seen in all compositions, consistent with previous studies highlighting its role in enhancing osteointegration [31, 45].

Mechanical testing

Mechanical properties were evaluated to determine the effect of varying PVA-OPP ratios on scaffold performance (Fig. 4). The tensile strength results (Fig. 4a) show that the 1PVA/0OPP/HAp scaffolds exhibited the highest tensile strength (3.31 ± 1.05 MPa), which can be attributed to strong hydrogen bonding between hydroxyl groups of PVA and surface functional groups of HAp particles. Such interactions enhance stress transfer efficiency and promote uniform load distribution within the polymer matrix [46]. This result is consistent with previous studies reporting excellent mechanical reinforcement ability of HAp in polymer matrices [47, 48]. However, the addition of OPP significantly reduced the tensile strength, with the 1PVA/1OPP/HAp scaffolds providing a severe reduction (0.30 ± 0.07 MPa), possibly due to poor interfacial adhesion between the lignocellulosic OPP particles and hydrophilic PVA matrix. Limited hydrogen bonding and weak interfacial adhesion at the molecular level can lead to stress concentration points and microstructural discontinuities, thereby deteriorating mechanical performance [49]. 2PVA/5OPP/HAp and

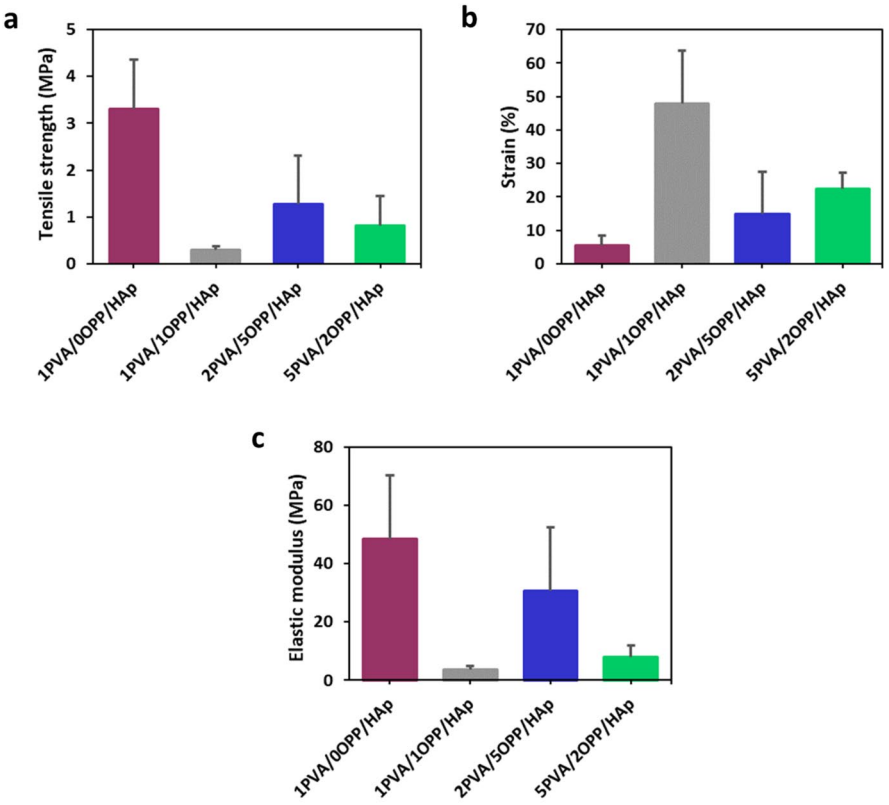


Fig. 4 Mechanical characterization of 3D-printed 1PVA/0OPP/HAp, 1PVA/1OPP/HAp, 2PVA/5OPP/HAp, and 5PVA/2OPP/HAp scaffolds: (**a**) tensile strength, (**b**) strain (%), and (**c**) elastic modulus of the scaffolds. Data are expressed as mean ± standard deviation (SD, $n = 3$)

5PVA/2OPP/HAp scaffolds showed moderate improvement in strength (1.27 ± 1.03 MPa and 0.82 ± 0.63 MPa, respectively), which may be related to the partial recovery of mechanical cohesion by improving matrix continuity with increasing PVA content. Moreover, strain at break values followed an opposite trend (Fig. 4b). The results clearly reveal that the 1PVA/1OPP/HAp formulation exhibited the highest elongation (47.9 ± 15.9%) and significantly outperformed all other groups in terms of ductility. This behavior can be attributed to reduced effective crosslink density and increased free volume within the composite, allowing greater polymer chain mobility under tensile loading. In contrast, both the 2PVA/5OPP/HAp and 5PVA/2OPP/HAp groups showed moderate strain values (14.8 ± 12.5% and 22.5 ± 4.7%, respectively). The absence of OPP in the 1PVA/0OPP/HAp scaffold resulted in the lowest strain value (5.5 ± 2.8%), possibly leading to a more rigid and brittle structure dominated by HAp with limited chain mobility. The elastic modulus data (Fig. 4c) exhibit that the 1PVA/0OPP/HAp scaffolds had the highest stiffness (48.4 ± 21.9 MPa), which is expected due to the mineral reinforcement provided by HAp and the absence of softening agents such as OPP. The addition of OPP again led to a significant reduction in modulus, with 1PVA/1OPP/HAp showing minimal stiffness (3.8 ± 1.1 MPa), highlighting the brittleness brought about by weakened intermolecular bonding, inadequate filler distribution, and potential pore formation. The 2PVA/5OPP/HAp and 5PVA/2OPP/HAp formulations demonstrated moderate stiffness values (30.8 ± 21.7 MPa and 7.9 ± 4.1 MPa, respectively), supporting the role of polymer concentration in modulating molecular connectivity and mechanical behavior [50]. The mechanical trends observed are also indicative of the scaffold's degradation behavior, as physically crosslinked PVA systems with lower crosslink density generally exhibit enhanced flexibility but faster hydrolytic degradation. The inclusion of OPP further modulates this behavior by increasing free volume and water uptake, while HAp contributes to structural stabilization, suggesting a balanced degradation profile suitable for early bone regeneration stages [51].

Reported tensile strength values for PVA/HAp scaffolds produced by freeze-drying generally range from ~ 0.1–1.5 MPa and are often accompanied by high brittleness due to their irregular pore structure [52, 53]. Electrospun PVA/HAp mats, on the other hand, generally exhibit improved tensile strength but lack 3D structural integrity and load-bearing capacity [54, 55]. In the present study, 3D-printed PVA/OPP/HAp scaffolds exhibited a balanced combination of strength and flexibility, achieving tensile strengths up to 3.31 ± 1.05 MPa while maintaining tunable ductility. Moreover, the introduction of OPP as a bio-based modifier provides an additional degree of freedom for tailoring mechanical behavior at both the molecular and structural levels, which is difficult to achieve using conventional fabrication routes.

MTT assay

The cell viability values of the obtained scaffolds were evaluated by performing the MTT analysis. In the research, the effects of PVA/OPP/HAp-based scaffolds containing different ratios of OPP on osteoblast cell viability were tested on the 1st, 3rd, and 7th days (Fig. 5). 2D culture medium was used as a reference value in terms of cell proliferation and metabolic activity on the scaffolds. On the 7th day, the cell via-

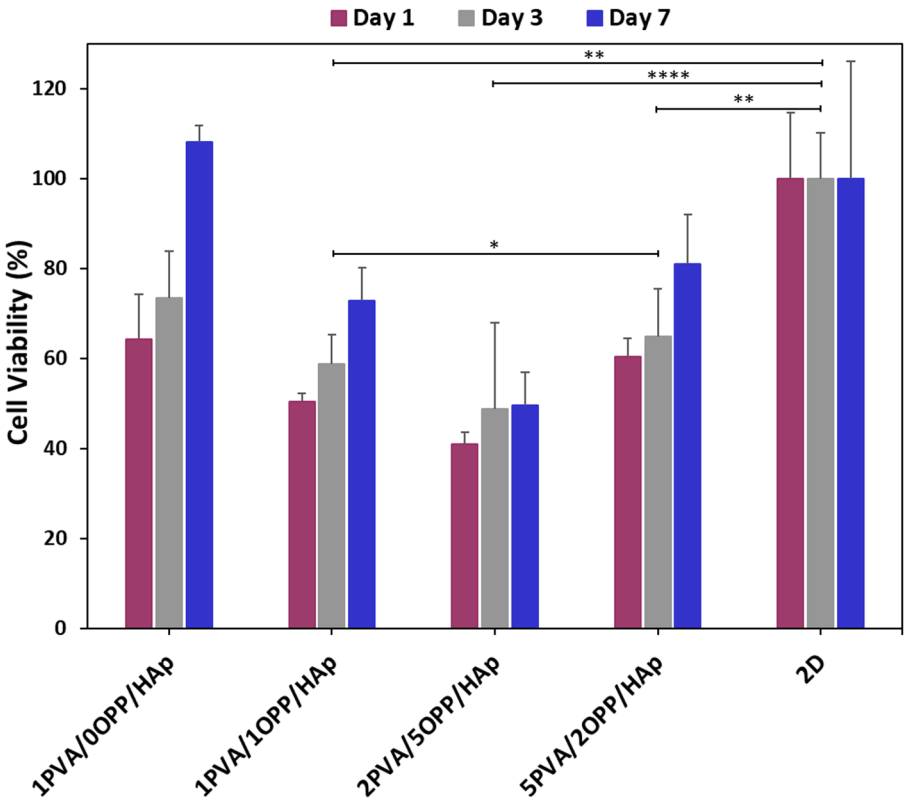


Fig. 5 Cell viability of the hFOB cell line cultured on 3D-scaffolds over the designated periods ($p<0.05$ (*), $p<0.01$ (**), $p<0.001$ (***), $p<0.0001$ (****))

bility values obtained from the 1PVA/0OPP/HAp, 1PVA/1OPP/HAp, 2PVA/5OPP/HAp, and 5PVA/2OPP/HAp scaffolds were measured as 108%, 72%, 49%, and 80%, respectively. An increasing cell viability rate was observed from day 1 to day 7 in the 1PVA/0OPP/HAp group without OPP. This increase can be proven by the biocompatibility of PVA and HAp and their support for cell proliferation [56, 57]. Although the viability rates were low in the first days in the 1PVA/1OPP/HAp and 5PVA/2OPP/HAp groups, it was observed that the viability increased during the incubation period. It is observed that the viability rates exceed 70%, especially on the 7th day. This situation can be said that the use of OPP at certain rates may initially create a slight toxic effect, but this effect decreases over time. It indicates that the phenolic compounds in the OPP content allow cell adaptation at low doses. A significant cytotoxicity was observed in the 2PVA/5OPP/HAp group. It is observed that cell viability increased to a maximum of 50% after the 7th day of incubation. The cytotoxic effects of high concentrations of phenolic compounds on cells are related to their shift from antioxidant to pro-oxidant behavior [58]. While phenolic compounds exhibit free radical scavenging effects at low doses, at high concentrations they can enter the redox cycle, leading to excessive production of intracellular reactive oxygen species (ROS) [59]. Increased ROS levels overcome the cell's antioxidant defense mechanisms, leading

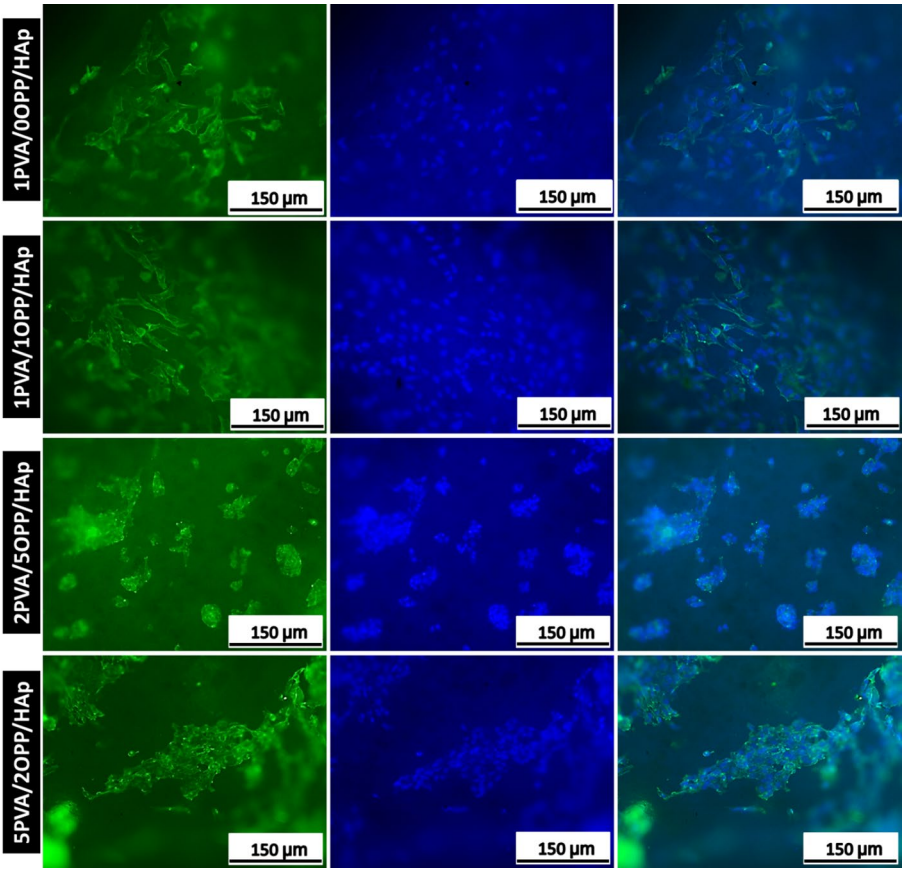


Fig. 6 Fluorescence microscopy images of 3D-printed 1PVA/0OPP/HAp, 1PVA/1OPP/HAp, 2PVA/5OPP/HAp, and 5PVA/2OPP/HAp scaffolds. The fixed cells were stained with DAPI (blue) and phalloidin (green) dye

to oxidative stress; this results in lipid peroxidation, protein oxidation, and DNA damage. The loss of mitochondrial membrane potential, decreased ATP production, and activation of caspase-mediated apoptotic pathways triggered by oxidative stress cause a significant decrease in cell viability [58, 60]. It can be said that high phenolic contents of various olive by-products, such as oleuropein and hydroxytyrosol, increase the production of ROS [61]. Similar to the literature, the results obtained show that scaffolds containing high levels of OPP suppress cell proliferation, while the phenolic compounds within them increase the production of ROS at high doses, leading to cell death. The increased amount of ROS may have caused oxidative stress by causing damage to DNA, increasing cell death, and causing higher toxicity [62, 63]. According to the results obtained, it can be seen that OPP can support biological activity when used at optimum doses, while its use at high concentrations causes cell death. It can be said that scaffolds containing OPP can provide biocompatible results depending on the dose in bone tissue engineering.

Fluorescence microscopy analysis

To assess the density and spread of hFOB cells on the scaffolds, nuclear DNA and actin staining were performed using DAPI (blue) and phalloidin (green) and the obtained fluorescence images are given in Fig. 6. According to the images obtained after 3 days of incubation, it can be said that cell spreading and proliferation were higher on 1PVA/0OPP/HAp and 1PVA/1OPP/HAp scaffolds. It can be said that hFOB cells especially showed a homogeneous spread on the scaffold surface. When 2PVA/5OPP/HAp and 5PVA/2OPP/HAp scaffolds were examined, it was observed that the cells did not spread homogeneously but proliferated in clusters. This situation was observed more in the 2PVA/5OPP/HAp scaffold in particular. The high phenolic compound-related stress prevented the cells from spreading. In addition, the high phenolic content of OPP may disrupt the pH balance of the medium, preventing cells from dispersing and spreading [4]. The images obtained were supportive of the cell viability results.

Although osteogenic differentiation markers and mineralization were not assessed in this study, the observed cell viability, spreading, and cytoskeletal organization on optimized OPP-containing scaffolds strongly suggest a supportive microenvironment for osteoblast function [51]. Previous studies have demonstrated that HAp-containing, porous scaffolds with moderate surface roughness promote osteogenic differentiation even in the absence of additional biochemical cues [64, 65]. In conclusion, these findings suggest that at specific concentrations, OPP can be incorporated into the scaffold without compromising cell viability, allowing cells to adapt to the microenvironment and maintain normal morphology and function.

Conclusion

This study demonstrates the potential of using agricultural waste, especially OPP, as a functional component in 3D-printed composite scaffolds for bone tissue engineering. Combinations of PVA, OPP, and HAp were successfully fabricated using an extrusion-based 3D printing technique. FTIR analysis confirmed the successful incorporation of each component, while SEM imaging revealed that increased OPP content improved scaffold porosity and surface roughness properties, which are known to promote osteogenesis. Mechanical tests showed that although high OPP concentrations may compromise tensile strength and stiffness, an optimal balance can retain sufficient structural integrity while improving ductility. In vitro evaluation through MTT assay and fluorescence microscopy revealed that low to moderate levels of OPP support osteoblast viability and adhesion, whereas excessive incorporation led to reduced cell proliferation, likely due to the oxidative effects of phenolic compounds. Overall, the findings indicate that OPP can be effectively integrated into scaffold formulations at controlled ratios to produce environmentally friendly, biocompatible, and structurally appropriate scaffolds. These results open new avenues for the valorization of agricultural waste in regenerative medicine and highlight the promise of green biomaterial strategies in developing next-generation bone graft substitutes.

Acknowledgements The authors would like to sincerely thank Biolive (Istanbul, Türkiye) for providing the olive pit powder used in this study.

Author contributions M. B. J.: Methodology; Investigation; Writing – Original Draft.G.U., Z. D. C., A.O.: Methodology, Investigation.T.B.: Supervision; Validation; Writing – Original Draft.S. S. T.: Project Administration.E.I.: Visualization; Writing – Original Draft.O.G.: Conceptualization; Supervision; Writing – Review & Editing. All authors reviewed the manuscript.

Funding Open access funding provided by the Scientific and Technological Research Council of Türkiye (TÜBİTAK).

Data availability No datasets were generated or analysed during the current study.

Declarations

Conflict of interest The authors declare no competing interests.

Open Access This article is licensed under a Creative Commons Attribution 4.0 International License, which permits use, sharing, adaptation, distribution and reproduction in any medium or format, as long as you give appropriate credit to the original author(s) and the source, provide a link to the Creative Commons licence, and indicate if changes were made. The images or other third party material in this article are included in the article's Creative Commons licence, unless indicated otherwise in a credit line to the material. If material is not included in the article's Creative Commons licence and your intended use is not permitted by statutory regulation or exceeds the permitted use, you will need to obtain permission directly from the copyright holder. To view a copy of this licence, visit http://creativecommons.org/licenses/by/4.0/.

References

1. Huang L, Wang J, Xu J et al (2025) Ferroptosis in osteogenic differentiation: a narrative review of bone regeneration metabolism. Regen Med Rep. https://doi.org/10.4103/regenmed.regenmed-d-25-00007
2. Wasilczyk C, Wasilczyk B (2024) Nanosurgery and bioengineered structural regenerative protocols for the treatment of human knee meniscal tears: a double-blind randomized controlled study of a novel regenerative method. Regen Med Rep. https://doi.org/10.4103/regenmed.regenmed-d-24-00015
3. Xue N, Ding X, Huang R et al (2022) Bone tissue engineering in the treatment of bone defects. Pharmaceuticals 15:879. https://doi.org/10.3390/ph15070879
4. Obied HK, Allen MS, Bedgood DR et al (2005) Bioactivity and analysis of biophenols recovered from Olive mill waste. J Agric Food Chem 53:823–837. https://doi.org/10.1021/jf048569x
5. De Pace R, Molinari S, Mazzoni E, Perale G (2025) Bone Regeneration: a review of current treatment strategies. J Clin Med. https://doi.org/10.3390/jcm14061838
6. Dimitriou R, Jones E, McGonagle D, Giannoudis PV (2011) Bone regeneration: current concepts and future directions. BMC Med 9:66. https://doi.org/10.1186/1741-7015-9-66
7. Hamza HM, Malik M, Asad M et al (2025) Advances in orthopedic implants: the role of nanotechnology in enhancing performance and longevity. Regen Med Rep 2:15–21. https://doi.org/10.4103/REGENMED.REGENMED-D-24-00024
8. Ferraz MP (2023) Bone Grafts in Dental Medicine: an overview of autografts, allografts and synthetic materials. Materials. https://doi.org/10.3390/ma16114117
9. Feroz S, Cathro P, Ivanovski S, Muhammad N (2023) Biomimetic bone grafts and substitutes: a review of recent advancements and applications. Biomedical Eng Adv 6:100107. https://doi.org/10.1016/j.bea.2023.100107

10. Selim M, Mousa HM, Khan MUA et al (2024) Enhancing 3D scaffold performance for bone tissue engineering: A comprehensive review of modification and functionalization strategies. J Science: Adv Mater Devices 9:100806. https://doi.org/10.1016/j.jsamd.2024.100806
11. Bose S, Roy M, Bandyopadhyay A (2012) Recent advances in bone tissue engineering scaffolds. Trends Biotechnol 30:546–554. https://doi.org/https://doi.org/https://doi.org/10.1016/j.tibtech.2012.07.005
12. Karageorgiou V, Kaplan D (2005) Porosity of 3D biomaterial scaffolds and osteogenesis. Biomaterials 26:5474–5491. https://doi.org/https://doi.org/https://doi.org/10.1016/j.biomaterials.2005.02.002
13. Zhu N, Che X (2013) Biofabrication of Tissue Scaffolds. Advances in Biomaterials Science and Biomedical Applications. InTech
14. Bedir T, Ulag S, Ustundag CB, Gunduz O (2020) 3D Bioprinting applications in neural tissue engineering for spinal cord injury repair. Mater Sci Eng C 110:110741. https://doi.org/10.1016/j.msec.2020.110741
15. Dananjaya V, Chevali V, Dear J et al (2024) 3D printing of biodegradable polymers and their composites – current state-of-the-art, properties, applications, and machine learning for potential future applications. Prog Mater Sci. https://doi.org/10.1016/j.pmatsci.2024.101336
16. Huang D, Li Z, Li G et al (2025) Biomimetic structural design in 3D-printed scaffolds for bone tissue engineering. Mater Today Bio 32:101664. https://doi.org/10.1016/j.mtbio.2025.101664
17. Mishra B, Mohanta YK, Reddy CN et al (2023) Valorization of agro-industrial biowaste to biomaterials: an innovative circular bioeconomy approach. Circ Econ 2:100050. https://doi.org/10.1016/j.cec.2023.100050
18. Burgos Pintos P, Maturi M, de León A, Molina SI (2024) Development of polymer composites using Surface-Modified Olive pit powder for fused granular fabrication. Polym (Basel) 16. https://doi.org/10.3390/polym16212981
19. Valvez S, Maceiras A, Santos P, Reis PNB (2021) Olive stones as filler for polymer-based composites: a review. Materials. https://doi.org/10.3390/ma14040845
20. Ciastowicz Ż, Pamuła R, Białowiec A (2024) Utilization of plant oils for sustainable polyurethane adhesives: a review. Materials. https://doi.org/10.3390/ma17081738
21. Ncube A, Mtetwa S, Bukhari M et al (2023) Circular economy and green chemistry: the need for radical innovative approaches in the design for new products. Energies 16:1752. https://doi.org/10.3390/en16041752
22. Bedir T, Baykara D, Yildirim R et al (2024) Three-dimensional-printed GelMA-KerMA composite patches as an innovative platform for potential tissue engineering of tympanic membrane perforations. Nanomaterials 14:563. https://doi.org/10.3390/nano14070563
23. Oun AA, Shin GH, Rhim J-W, Kim JT (2022) Recent advances in polyvinyl alcohol-based composite films and their applications in food packaging. Food Packag Shelf Life 34:100991. https://doi.org/10.1016/j.fpsl.2022.100991
24. Gülel Ş, Güvenilir Y (2024) Olive stone powder filled bio-based polyamide 5.6 biocomposites: biodegradation in natural soil and mechanical properties. Polym Bull 81:14385–14410. https://doi.org/10.1007/s00289-024-05388-6
25. Wang Z, Chu Y, Du J et al (2024) Accelerating repair of infected bone defects through post-reinforced injectable hydrogel mediated antibacterial/immunoregulatory microenvironment at bone-hydrogel interface. Carbohydr Polym 351:123082. https://doi.org/10.1016/j.carbpol.2024.123082
26. Arslan Tut T, Cesur S, Sahin A et al (2024) Production of platelet-rich plasma (PRP)-enriched scaffolds for bone tissue regeneration with 3D printing technology. Eur Polym J 219:113371. https://doi.org/10.1016/j.eurpolymj.2024.113371
27. Mondal S, Park S, Choi J et al (2023) Hydroxyapatite: a journey from biomaterials to advanced functional materials. Adv Colloid Interface Sci 321:103013. https://doi.org/10.1016/j.cis.2023.103013
28. Farjaminejad S, Farjaminejad R, Hasani M et al (2024) Advances and challenges in polymer-based scaffolds for bone tissue engineering: a path towards personalized regenerative medicine. Polymers. https://doi.org/10.3390/polym16233303
29. Radha G, Manjubaashini N, Balakumar S (2023) Nano-hydroxyapatite/natural polymer composite scaffolds for bone tissue engineering: a brief review of recent trend. Vitro Models 2:125–151. https://doi.org/10.1007/s44164-023-00049-w
30. Ashraf AA, Zebarjad SM, Hadianfard MJ (2019) The cross-linked polyvinyl alcohol/hydroxyapatite nanocomposite foam. J Mater Res Technol 8:3149–3157. https://doi.org/10.1016/j.jmrt.2019.02.024

31. Bozdag M, Urek F, Cesur S et al (2025) Bovine serum albumin (BSA)-loaded polyvinyl alcohol (PVA) / chitosan (CH) / hydroxyapatite (HA) electrospun nanofibers for bone tissue regeneration. J Drug Deliv Sci Technol 106:106712. https://doi.org/10.1016/j.jddst.2025.106712
32. Nouri S, Roghanian R, Emtiazi G et al (2024) The efficacy of probiotic mediated hydroxyapatite in mammalian cell culture: promotion of MG–63 and L–929, anti–MCF7 breast cancer cells activities, and cytokine production of PBMC. Emergent Mater. https://doi.org/10.1007/s42247-024-00828-5
33. Calovi M, Rossi S (2023) Olive pit powder as multifunctional pigment for waterborne paint: influence of the bio-based filler on the aesthetics, durability and mechanical features of the polymer matrix. Ind Crops Prod 194:116326. https://doi.org/10.1016/j.indcrop.2023.116326
34. Ghavidel A, Bak M, Hofmann T et al (2021) Evaluation of some wood-water relations and chemometric characteristics of recent oak and archaeological oak wood (*Quercus robur*) with archaeometric value. J Cult Heritage 51:21–28. https://doi.org/10.1016/J.CULHER.2021.06.011
35. Ghavidel A, Hosseinpourpia R, Gelbrich J et al (2021) Microstructural and chemical characteristics of archaeological white elm (*Ulmus laevis* P.) and poplar (*Populus* spp.). Appl Sci. https://doi.org/10.3390/app112110271
36. Bedir T, Baykara D, Sahin A et al (2024) Development of specially designed nanoparticle-coated 3D-printed gelatin methacryloyl patches for potential tissue engineering applications. Macromol Mater Eng 2400199. https://doi.org/10.1002/mame.202400199
37. Choo K, Ching YC, Chuah CH et al (2016) Preparation and characterization of polyvinyl alcohol-chitosan composite films reinforced with cellulose nanofiber. Materials. https://doi.org/10.3390/ma9080644
38. Kubo S, Kadla JF (2003) The formation of strong intermolecular interactions in immiscible blends of poly(vinyl alcohol) (PVA) and lignin. Biomacromolecules 4(3):561–7
39. Szatkowski T, Kołodziejczak-Radzimska A, Zdarta J et al (2015) SYNTHESIS AND CHARACTERIZATION OF HYDROXYAPATITE/CHITOSAN COMPOSITES. Physicochemical Probl Mineral Process 51:575–585
40. Zhang Q, Yu Z, Jin S et al (2020) Role of surface roughness in the algal short-term cell adhesion and long-term biofilm cultivation under dynamic flow condition. Algal Res 46:101787. https://doi.org/10.1016/j.algal.2019.101787
41. Marcuello C, Chabbert B, Berzin F et al (2023) Influence of surface chemistry of fiber and lignocellulosic materials on adhesion properties with polybutylene succinate at nanoscale. Materials. https://doi.org/10.3390/ma16062440
42. Głąb M, Drabczyk A, Kudłacik-Kramarczyk S et al (2022) Investigations on the influence of collagen type on physicochemical properties of PVP/PVA composites enriched with hydroxyapatite developed for biomedical applications. Materials 15. https://doi.org/10.3390/ma15010037
43. Mukasheva F, Adilova L, Dyussenbinov A et al (2024) Optimizing scaffold pore size for tissue engineering: insights across various tissue types. Front Bioeng Biotechnol 12:1444986. https://doi.org/10.3389/fbioe.2024.1444986
44. Lee JH, Jang HL, Lee KM et al (2013) In vitro and in vivo evaluation of the bioactivity of hydroxyapatite-coated polyetheretherketone biocomposites created by cold spray technology. Acta Biomater 9:6177–6187. https://doi.org/10.1016/j.actbio.2012.11.030
45. Codrea CI, Baykara D, Mitran R-A et al (2024) 3D-bioprinted gelatin methacryloyl-strontium-doped hydroxyapatite composite hydrogels scaffolds for bone tissue regeneration. Polymers. https://doi.org/10.3390/polym16131932
46. Mollazadeh S, Javadpour J, Khavandi A (2007) Biomimetic synthesis and mechanical properties of hydroxyapatite/poly (vinyl alcohol) nanocomposites. Adv Appl Ceram 106:165–170
47. Wu Y, Yang Z, Madiyar F et al (2025) Hydroxyapatite functionalized natural fiber-reinforced composites: interfacial modification and additive manufacturing. Polym Compos 46:141–155. https://doi.org/10.1002/pc.28974
48. Poursamar SA, Orang F, Bonakdar S, avar M (2010) Preparation and characterisation of Poly vinyl alcohol/hydroxyapatite nanocomposite via in situ synthesis: a potential material as bone tissue engineering scaffolds. Int J Nanomanuf 5:330
49. Kun D, Kárpáti Z, Fekete E, Móczó J (2021) The role of interfacial adhesion in polymer composites engineered from lignocellulosic agricultural waste. Polymers (Basel). https://doi.org/10.3390/polym13183099
50. Anandan D, Stella SM, Nambiraj NA et al (2018) Development of mechanically compliant 3D composite scaffolds for bone tissue engineering applications. J Biomed Mater Res A 106(12):3267–3274

51. Du J, Chu Y, Hu Y et al (2024) A multifunctional self-reinforced injectable hydrogel for enhancing repair of infected bone defects by simultaneously targeting macrophages, bacteria, and bone marrow stromal cells. Acta Biomater 189:232–253. https://doi.org/10.1016/j.actbio.2024.10.014
52. Xiang C, Zhang X, Zhang J et al (2022) A porous hydrogel with high mechanical strength and biocompatibility for bone tissue engineering. J Funct Biomater. https://doi.org/10.3390/jfb13030140
53. Zhou X-H, Wei D, Ye H et al (2016) Development of poly(vinyl alcohol) porous scaffold with high strength and well ciprofloxacin release efficiency. Mater Sci Eng C Mater Biol Appl 67:326–335
54. Farsi M, Asefnejad A, Baharifar H (2022) A hyaluronic acid/PVA electrospun coating on 3D printed PLA scaffold for orthopedic application. Prog Biomater 11:67–77
55. Hartatiek Y, Wuriantika MI et al (2021) Nanostructure, porosity and tensile strength of PVA/Hydroxyapatite composite nanofiber for bone tissue engineering. Mater Today Proc
56. Cesur S, Ilhan E, Pilavci E et al (2023) A novel strategy as a potential rapid therapy modality in the treatment of corneal ulcers: fluconazole/vancomycin dual drug-loaded nanofibrous patches. Macromol Mater Eng 308:2200697. https://doi.org/10.1002/mame.202200697
57. Trzaskowska M, Vivcharenko V, Benko A et al (2024) Biocompatible nanocomposite hydroxyapatite-based granules with increased specific surface area and bioresorbability for bone regenerative medicine applications. Sci Rep 14:28137. https://doi.org/10.1038/s41598-024-79822-0
58. Galati G, O'Brien PJ (2004) Potential toxicity of flavonoids and other dietary phenolics: significance for their chemopreventive and anticancer properties. Free Radic Biol Med 37:287–303. https://doi.org/10.1016/j.freeradbiomed.2004.04.034
59. Scalbert A, Johnson IT, Saltmarsh M (2005) Polyphenols: antioxidants and beyond2. Am J Clin Nutr 81:215S–217. https://doi.org/10.1093/ajcn/81.1.215S. S
60. Halliwell B (2007) Dietary polyphenols: good, bad, or indifferent for your health? Cardiovasc Res 73:341–347. https://doi.org/10.1016/j.cardiores.2006.10.004
61. Centrone M, D'Agostino M, Difonzo G et al (2020) Antioxidant efficacy of olive by-product extracts in human colon HCT8 cells. Foods. https://doi.org/10.3390/foods10010011
62. Anantharaju PG, Gowda PC, Vimalambike MG, Madhunapantula SV (2016) An overview on the role of dietary phenolics for the treatment of cancers. Nutr J 15:99. https://doi.org/10.1186/s12937-016-0217-2
63. Park WH (2013) Effects of antioxidants and MAPK inhibitors on cell death and reactive oxygen species levels in H(2)O(2)-treated human pulmonary fibroblasts. Oncol Lett 5:1633–1638. https://doi.org/10.3892/ol.2013.1216
64. Acharya R, Dutta SD, Patil TV et al (2025) 3D-printed magnesium/nanodiamond dual-doped hydroxyapatite composite hydrogels with antibacterial and in vitro bioactive properties for bone tissue engineering. J Am Ceram Soc 108. https://doi.org/10.1111/jace.70121
65. Yang W, Han W, He W et al (2016) Surface topography of hydroxyapatite promotes osteogenic differentiation of human bone marrow mesenchymal stem cells. Mater Sci Eng C Mater Biol Appl 60:45–53

Publisher's note Springer Nature remains neutral with regard to jurisdictional claims in published maps and institutional affiliations.

Authors and Affiliations

Mohamed Bella Jagitay[1,2] · Gulpembe Ustundag[1,3] · Zehra Desen Celik[1,4] · Ayse Onur[1,5] · Tuba Bedir[1] · Sena Su Torun[1,6] · Elif Ilhan[1] · Oguzhan Gunduz[1,7]

✉ Tuba Bedir
tuba.bedir@marmara.edu.tr

[1] Center for Nanotechnology & Biomaterials Application and Research (NBUAM), Marmara University, Istanbul, Turkey

[2] Department of Bioengineering, Faculty of Engineering and Natural Sciences, Uskudar University, Istanbul, Turkey

[3] Aljazari International Schools of Science and Technology, Istanbul, Turkey

[4] Department of Molecular Biology, Cell Biology, and Biochemistry, Brown University, Providence, USA

[5] Sakıp Sabancı Anatolian High School, Istanbul, Turkey

[6] Department of Bioengineering, Faculty of Chemistry and Metallurgy, Yildiz Technical University, Istanbul, Turkey

[7] Department of Metallurgical and Materials Engineering, Faculty of Technology, Marmara University, Istanbul, Turkey